RSC Advances

PAPER

Cite this: *RSC Adv.*, 2021, **11**, 20570

Ru–Ni bimetallic catalysts for steam reforming of xylene: effects of active metals and calcination temperature of the support

Jianglong Pu, *[ab] Hui Wang,[a] Masayuki Suzuki[b] and Eika W. Qian *[b]

A series of Ru and Ni supported catalysts were prepared and their catalytic performance was evaluated in the steam reforming of xylenes. The effects of active metals, active metal loading sequence, and the calcination temperature of the support on the catalyst activity and stability were investigated. The bimetallic 2Ru → 15Ni catalyst shows much higher activity and stability than the monometallic 2Ru and 15Ni catalyst owing to the synergic effect of Ni and Ru. The 2Ru → 15Ni catalyst has the least coke deposition owing to its high conversion performance and much less coke precursor being formed on the catalyst surface. After decoking, most of the small-sized pores cannot be recovered because of the pore collapse under severe hydrothermal conditions. *o*-Xylene has the lowest reactivity due to electronic and steric effects. Besides the steam reforming reaction, demethylation and C–C cracking are also observed, forming benzene and toluene. The catalyst with a loading sequence of 15Ni → 2Ru shows high activity at low temperatures (550–600 °C), but undergoes an activity drop at high temperatures (625–650 °C) because the Ni sintering at high temperatures greatly affects the state of Ru on the catalyst. The catalyst with a loading sequence of 2Ru → 15Ni has an advantage at high temperatures owing to its better sintering resistance. The simultaneously loaded 2Ru ↔ 15Ni catalyst shows the lowest activity. The high calcination temperature of the support enhances the catalyst stability by eliminating the small-sized pores before reaction; on the other hand, the elimination of pores decreases the dispersion of the active metals. The 2Ru → 15Ni catalyst calcined at 1000 °C balances the active metal dispersion and resistance to sintering under severe hydrothermal conditions, showing the best activity and stability. The catalyst calcined at 1000 °C has the best coke resistance with only 0.166 g g_{cat}^{-1} of coke formation after the 24 h durability test. The DTG results indicate that the carbon formed on the catalysts is mainly graphitic carbon.

Received 13th April 2021
Accepted 28th May 2021

DOI: 10.1039/d1ra02864b

rsc.li/rsc-advances

1. Introduction

Recently, fuel cells with hydrogen have received extensive attention in the field of electric vehicles[1,2] and are expected to replace conventional combustion engines owing to their pollution-free, high-efficiency, and renewable characters.[3] The steam reforming of bio-oil is an efficient approach to produce hydrogen because of the abundant biomass on the earth that can be renewed by the photosynthesis of the plant.[4] The source of biomass and conditions of pyrolysis determine the composition of bio-oil, including water, organic acids, alcohols, esters, phenols, and other oligomers,[5] which are derived from the depolymerization of cellulose and lignin in the biomass.[4] The complex compositions of bio-oil make the hydrogen production *via* steam reforming of bio-oil a great challenge due to the different reactivities of each compound.[4] The high operating temperature and steam/carbon ratio can achieve a high hydrogen yield, while this will consume a large amount of energy and the severe hydrothermal conditions will lead to the metal sintering of the catalyst. Moreover, the oxygen-containing compounds in the bio-oil result in the deactivation of the catalyst easily because of the coke deposition.[6,7] Therefore, a catalyst with good catalytic activities and stabilities towards all kinds of compounds is the key to convert bio-oil into hydrogen in this process.

The catalytic activity and stability are dependent on the metal type, metal dispersion, properties and structures of supports, and interactions between metals and supports.[8,9] Both noble metal-supported catalysts (Pt, Ru, Pd, *etc.*) and transition metal-supported catalysts[10,11] (Ni, Co, Cu, *etc.*) are usually designed for the steam reforming reactions due to their superior ability to cleave C–C and C–H bonds.[12] High catalytic activities and hydrogen selectivity could be achieved over the noble metal-supported catalysts with a small metal loading

[a]*College of Biological, Chemical Sciences and Engineering, Jiaxing University, 118 Jiahang Road, Jiaxing 314001, China. E-mail: longpu@zjxu.edu.cn*
[b]*Graduate School of Bio-Applications and Systems Engineering, Tokyo University of Agriculture and Technology, 2-24-16, Nakacho, Koganei, Tokyo 184-8588, Japan. E-mail: whqian@cc.tuat.ac.jp*

amount, while their high cost and high sensitivity to the poison become a great barrier to their application. In contrast, the transition metal-supported catalysts have more potential for industrial utilization because of the low cost and relatively high activity if the loading amount is high.[13,14] However, both two types of catalysts have deactivation problems derived from metal sintering and carbon deposition, notably in the case of Ni-based catalysts.[15] Catalyst activity and stability can be enhanced by employing the bimetallic catalyst owing to the synergic effect, formation of alloy, and improvement of metal dispersion.[15–19] Ishihara *et al.* studied the Ni–Ru bimetallic catalyst in the steam reforming of cresol and found that the Ru added Ni-based catalysts exhibited much higher activity and stability than the monometallic Ni catalyst owing to the formation of Ni–Ru clusters.[16] The well-dispersed metals not only improve the catalyst activity owing to the increased contact surface of the active sites but also enhance the catalyst stability by forming strong metal–support interaction.[20] Moreover, the strong metal–support interaction changes the metal form and valence electron state, forming new active sites, which are favorable to the steam reforming reactions.[21] The supports play a crucial role in improving the catalytic activity and stability since they not only support the active sites but also participate in the reactions by strengthening the catalyst's ability to dissociate water.[16,22] Alumina is suitable for catalyst support in steam reforming reactions because it is hydrothermally stable and has a strong water dissociation ability.[6] However, the acid sites on the alumina support accelerate the dehydration reactions forming the undesirable coke, thus the support is usually modified by other oxides. The loading of alkaline oxides such as MgO, BaO, and CaO can neutralize the acid sites and inhibit the coke formation,[23–26] while strong alkalinity induced by Na or Mg will also decrease the catalytic performance by forming some oxygen-containing species.[27] The loading of oxides with oxygen storage capacity and facile redox properties such as CeO_2 can facilitate the removal of coke owing to their mobile lattice oxygen.[5,13] During the steam reforming reactions, La_2O_3 shows superior decoking ability because it can absorb CO_2, forming oxycarbonate that oxidizes carbon into CO,[12,28,29] and on the other hand, the addition of La_2O_3 can enhance the Ni dispersion and increase the alkalinity to a mild extent, which are favorable to the catalytic performance and coke resistance of the catalyst.[27,29–31]

Although the steam reforming of bio-oil using small molecules has been extensively studied, the catalyst study based on the large-molecule aromatic compounds is limited but meaningful because of the easy coke formation.[16] The major challenge in the steam reforming of lignin-derived oil is the catalyst deactivation caused by coke deposition. One strategy is to enhance the steam adsorption capability to gasify coke or coke precursor on the catalyst. The incorporation of alkaline oxides such as MgO and CaO not only promotes the steam adsorption ability of the catalyst but also decreases the acidic sites on the alumina support which can catalyze the carbon formation during steam reforming reactions.[32,33] The other strategy is to modify the surface reactions by loading other oxides. La_2O_3 was observed to enable the removal of carbon by forming oxycarbonate intermediates with CO_2.[12,28,29]

Based on these results, we designed the $5La_2O_3$–$10MgO$–Al_2O_3 support to improve the steam adsorption capability and incorporate decoking surface reactions, aiming at enhancing the coke resistance of the catalyst in the steam reforming of xylenes (consist of *o*-xylene, *p*-xylene, *m*-xylene, and ethylbenzene). Ni–Ru bimetal was employed as the active site to improve the catalytic activity of the catalyst. The catalytic performance in the steam reforming of xylenes was studied from the new viewpoints, *i.e.*, effects of porous structure alternation by changing the types of active metals, changing the metal loading sequence, changing support calcination temperature on the catalyst activity and stability. The relations between the pore structure and catalytic performance before and after the reaction were elucidated. The pore change derived from the coking and decoking process was focused.

2. Experimental

2.1 Materials

γ-Al_2O_3 (Nippon Ketjen, ≥99.0, 287 $m^2\ g^{-1}$), lanthanum(III) nitrate hexahydrate ($La(NO_3)_3 \cdot 6H_2O$, Kishida Reagents Chemicals), magnesium(II) nitrate hexahydrate ($Mg(NO_3)_2 \cdot 6H_2O$, Kishida Reagents Chemicals), nickel(II) nitrate hexahydrate ($Ni(NO_3)_2 \cdot 6H_2O$, Kishida Reagents Chemicals), ruthenium(III) chloride hydrate ($RuCl_3 \cdot (1–3)H_2O$, Kishida Reagents Chemicals) were received without further purification.

2.2 Catalyst preparation

γ-Al_2O_3 was crushed and sieved into the pellets (20–30 mesh) then calcined at 500 °C for 6 h before used. The catalyst support with 5 wt% La_2O_3 and 10 wt% MgO ($5La_2O_3$–$10MgO$–Al_2O_3) were prepared by the impregnation method. Typically, $La(NO_3)_3 \cdot 6H_2O$ and $Mg(NO_3)_2 \cdot 6H_2O$ aqueous solution were mixed with the calcined γ-Al_2O_3 pellets, then the water was vaporized slowly in the sand bath with gentle stirring. The catalyst supports were dried at 120 °C for 3 h and calcined at various temperatures (750 °C, 1000 °C, and 1100 °C) for 6 h.

The catalysts with 15 wt% Ni (designated as 15Ni) and 2 wt% Ru (designated as 2Ru) were prepared *via* impregnation method using $Ni(NO_3)_2 \cdot 6H_2O$ and $RuCl_3$ as precursors, respectively. The bimetallic catalysts were prepared using various methods: (i) 15 wt% Ni and 2 wt% Ru were loaded into the support successively (15Ni → 2Ru); (ii) 2 wt% Ru and 15 wt% Ni were loaded into the support successively (2Ru → 15Ni); (iii) 2 wt% Ru and 15 wt% Ni were simultaneously loaded into the support (2Ru ↔ 15Ni). In the case of (i) and (ii), a procedure of drying at 120 °C for 3 h was conducted before the second metal was loaded. Finally, all the catalysts were dried at 120 °C for 3 h.

2.3 Catalyst characterization

N_2 adsorption and desorption of the catalyst at liquid nitrogen temperature (−196 °C) were conducted in a Beckman Coulter analyzer (SA3100) to measure the BET surface area, pore

volume, and pore diameter distribution of the catalyst. Before analysis, the fresh catalysts were reduced at 600 °C for 3 h. All the samples were dried at 350 °C for 3 h with 50 mL min^{-1} N_2 flow, then outgassed at 300 °C for 1 h to remove the moisture.

Thermal gravimetric analysis (TGA) of the spent samples was conducted with a TA instrument (TGA, TA-60WS, SHIMADZU) to determine the carbon species formed on the catalyst. Approximately 10 mg of a sample was loaded to a platinum crucible and dried at 105 °C for 2 h. Subsequently, the sample was heated to 900 °C with a heating rate of 10 °C min^{-1} under 50 mL min^{-1} air flow. The coke amount of the spent catalyst was calculated according to the following equation:

$$W_{coke}\ (g\ g_{cat}^{-1}) = \frac{\text{weight of coked catalyst} - \text{weight of decoked catalyst}}{\text{weight of decoked catalyst}}$$

2.4 Catalytic activity

The catalyst evaluation was conducted in a fixed bed flow reactor (SSL316, φ 10 mm × 1 mm, 350 mm length). Approximately 0.50 g of the catalyst was diluted with quartz sand (Kishida Reagents Chemicals) and loaded into the constant-temperature zone of the reactor. Before the reaction, the catalyst was reduced by H_2 (50 mL min^{-1}) at 600 °C for 3 h. According to our preliminary experiment, the catalyst treated with water at 750 °C showed better catalytic performance than the case without a water treatment, which was probably attributed to the enhanced steam adsorption on the catalyst during the high-temperature water treatment. Therefore, in this study, after the H_2 reduction and before the activity test, all the catalysts were treated with H_2O (0.8 mL min^{-1}) at 750 °C for 3 h. Subsequently, water and mixtures of xylenes (62.92 wt% *p*- & *m*-xylene, 22.85 wt% *o*-xylene, and 14.23 wt% ethylbenzene) were continuously fed by two pumps with a molar ratio of steam to carbon of 3.4. Before getting into the reactor, water and xylenes were preheated to 400 °C. The reaction pressure was kept at 1.0 MPa. The residual liquid and the produced gas were separated using a cold trap in the outlet of the reactor. The gas flow rate was measured by a gas flow meter (Tokyo Shinagawa Corp.). The H_2 composition was quantified by GC-TCD (SHIMADZU, GC-8A, Prapack Q 2.0 m) using N_2 as carrier gas and the compositions of carbonaceous gas (CO, CH_4, and CO_2) were quantified by GC-TCD (SHIMADZU, GC-14B, Unibeads C 3.0 m) using He as carrier gas. The unreacted oil phase in the liquid was separated using a separatory funnel and analyzed by GC-FID (SHIMADZU, GC-14B, DB-1 60 m).

The conversion of the feedstock was calculated according to the equation below:

$$\text{Conversion}\ (\%) = \frac{\text{carbon in the feed} - \text{carbon in the unreacted oil}}{\text{carbon in the feed}} \times 100\%$$

The yield of H_2 was defined by the stoichiometric H_2 formation:

$$H_2\ \text{yield}\ (\%) = \frac{\text{moles of produced } H_2}{\text{theoretical moles of } H_2} \times 100\%$$

The yield of carbonaceous gas (CO, CH_4, and CO_2) was estimated on a carbon basis:

$$\text{Yield of CO, } CH_4, \text{ and } CO_2\ (\%) = \frac{\text{moles of CO, } CH_4, \text{ and } CO_2 \text{ in the gas}}{\text{moles of carbon in the feed}} \times 100\%$$

3. Results and discussion

3.1 Effect of active metals

The effect of active metals on the catalytic activity in the steam reforming of xylenes is investigated by loading Ni, Ru, and RuNi to the prepared $5La_2O_3$–$10MgO$–Al_2O_3 support. The pore structure, catalytic activity under various temperatures and weight hourly space velocity (WHSV), durability, and coke formation of the catalysts were systematically studied.

3.1.1 Pore structures. The pore size distributions of fresh 15Ni, 2Ru, 2Ru → 15Ni, and the $5La_2O_3$–$10MgO$–Al_2O_3 support are presented in Fig. 1. All the samples show similar pore diameter distributions and their pore sizes are concentrated at 5–15 nm. The bare support possesses the best porous structure and after the loading of active metals, the proportion of micropores decreases to a low level because of the partial obstruction by the metals. However, the proportion of the small-sized pore in the 2Ru catalyst is much larger than those of the 15Ni and 2Ru → 15Ni catalysts, indicating that the pore structure in 2Ru is well maintained due to the small loading amount of Ru. By contrast, the small-sized pore in 15Ni and 2Ru → 15Ni is partially obstructed by the large loading amount of Ni. Accordingly, the surface area and pore volume in 2Ru is much larger than those of 15Ni and 2Ru → 15Ni as listed in Table 1. No significant difference is observed in the pore

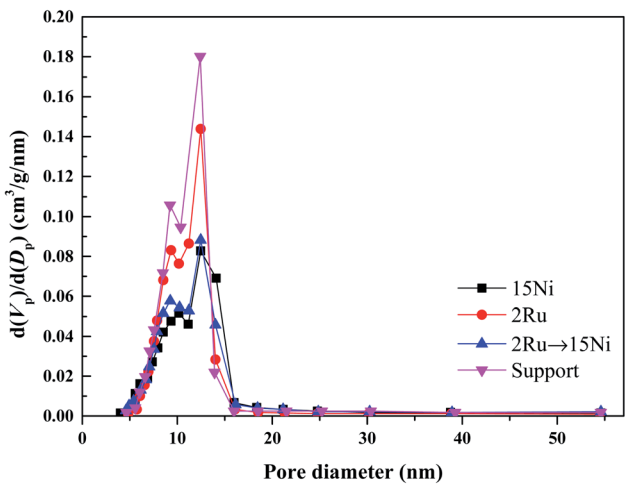

Fig. 1 Pore size distribution of catalysts (15Ni, 2Ru, and 2Ru → 15Ni) reduced at 600 °C and the support ($5La_2O_3$–$10MgO$–Al_2O_3) calcined at 750 °C.

Table 1 Coke amount, BET surface area, and pore volume of the catalysts with various active metals[a]

Catalyst		Surface area ($m^2\ g^{-1}$)	Pore volume ($cm^3\ g^{-1}$)	Coke ($g\ g_{cat}^{-1}$)
15Ni	Fresh	147	0.483	0.518
	Coked	60.8	0.197	
	Decoked	121	0.431	
2Ru	Fresh	184	0.576	0.462
	Coked	67.5	0.217	
	Decoked	120	0.404	
2Ru → 15Ni	Fresh	151	0.497	0.365
	Coked	65.5	0.302	
	Decoked	74.6	0.463	

[a] The supports of all the fresh catalysts were calcined at 750 °C for 6 h.

structures between the 15Ni and 2Ru → 15Ni catalysts. Interestingly, the 2Ru → 15Ni catalyst has a little more small-sized pores than 15Ni, showing larger pore volume and surface area. This suggests that the loading of Ru before Ni inhibits the Ni diffusion to the small-sized pore, thus more small-sized pores (5–10 nm) in 2Ru → 15Ni are maintained in comparison to 15Ni, as shown in Fig. 1.

3.1.2 Activity test. The yields of hydrogen, carbonaceous gas, and the unreacted oil in the steam reforming of xylenes under various reaction temperatures are shown in Fig. 2. The conversion of the feedstock and hydrogen yield increase with the rising temperature significantly since a high temperature is both kinetically and thermodynamically beneficial to the steam reforming reaction.[5] All the catalysts show low conversions and hydrogen yields at low temperatures (550–600 °C). An almost complete conversion of oil is observed over both 2Ru and 2Ru → 15Ni catalysts at 650 °C, indicating that 650 °C is required for the steam reforming of xylenes to get a considerable gas formation. For the monometallic catalysts, the hydrogen yield over the 15Ni catalyst is higher than that of the 2Ru catalyst below 625 °C, suggesting that Ni has better catalytic performance than Ru at low temperatures. Similar results were obtained by the previous study that the monometallic Ru catalyst seemed to not be effective for the steam reforming of cresol at low temperatures in comparison to the Ni-based catalyst.[16] However, above 625 °C much higher oil conversion and hydrogen yield are shown over the 2Ru catalyst, indicating that Ru has a great advantage in catalyzing the reaction at high temperatures. Kousi *et al.* studied the steam reforming of glycerol over the Ru catalysts and found that the products were dominated by the metallic activity at high temperatures, and by the acid–base properties on the support at low temperatures.[34] These observations suggest that a relatively high temperature is necessary for Ru active sites to effectively catalyze the steam reforming reaction. Nevertheless, the bimetallic 2Ru → 15Ni catalyst combines the advantages of 2Ru and 15Ni, showing the best catalytic performance at all the tested temperature points. The difference in hydrogen yield between 15Ni and 2Ru → 15Ni is not large at 550 °C, indicating that the working active metal in 2Ru → 15Ni at low temperatures is mainly Ni. At high temperatures, the 2Ru → 15Ni catalyst shows much higher activity than the monometallic catalysts owing to the synergic effect between Ru and Ni. Although 2Ru → 15Ni shows higher hydrogen yields at 550 °C and 575 °C, the oil conversions are lower than the monometallic catalysts. This may be explained by the less carbon formation over 2Ru → 15Ni as shown in Table 1, and part of the unreacted oil over the 15Ni catalyst is converted into carbon because of its easy carbon formation characters.[35] The addition of Ru is very effective for the inhibition of coke deposition in the steam reforming reactions due to the various surface reaction pathways.[36] At 650 °C, the 15Ni catalyst shows the worst activity and almost full conversions are obtained over both 2Ru and 2Ru → 15Ni, while the hydrogen yield over 2Ru is much lower (49.9%) than that of the 2Ru → 15Ni catalyst (59.2%). This suggests that the bimetallic 2Ru → 15Ni catalyst not only combines the advantages of Ni and Ru but

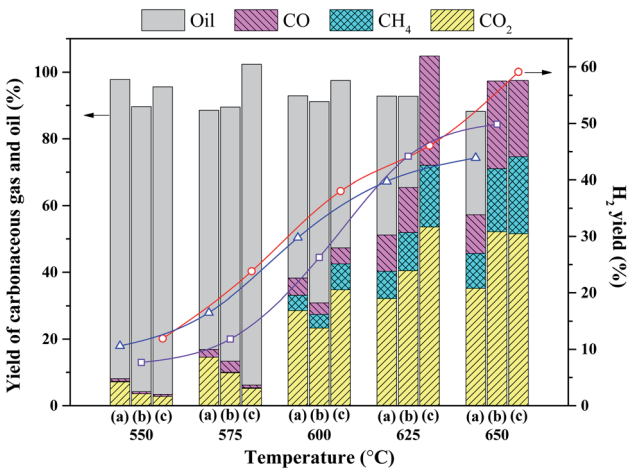

Fig. 2 Yields of hydrogen, carbonaceous gas, and oil in the steam reforming of xylene under various reaction temperatures over (a) 15Ni, (b) 2Ru, and (c) 2Ru → 15Ni. Reaction conditions: WHSV = 20.8 h^{-1}, S/C = 3.4, 1.0 MPa.

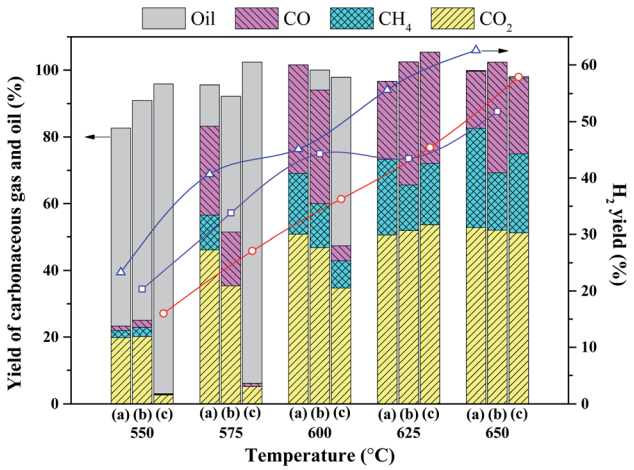

Fig. 3 Yields of hydrogen, carbonaceous gas, and oil in the steam reforming of xylene over 2Ru → 15Ni catalyst with a WHSV of (a) 10.4, (b) 15.6, and (c) 20.8 h^{-1}. Reaction conditions: S/C = 3.4, 1.0 MPa.

also exhibits a strong synergic effect that enhances the catalytic performance drastically.

To determine an appropriate WHSV for the reaction, the effect of WHSV on the catalytic performance of 2Ru → 15Ni under various reaction temperatures was investigated as shown in Fig. 3. A low WHSV will lead to a decrease in the production capacity, and on the other hand, less feed will pass through the catalyst bed per unit of time, thus the oil conversion and hydrogen yield will increase. The results indicate that the effect of WHSV at low temperatures is significant, while all cases reach full conversions above 625 °C and the reaction temperature becomes the dominant effect, thus the disparity in the hydrogen yield at 15.6 and 20.8 h^{-1} becomes small. At 600 °C, the oil conversion at 10.4 h^{-1} of WHSV reaches 100%, nevertheless, in the case of 20.8 h^{-1}, over 50% yield of oil is still left in the residual liquid. Therefore, to better compare the catalytic performance of various catalysts, a WHSV of 20.8 h^{-1} was selected for the latter activity and durability test in this study.

3.1.3 Durability test. The durability test of the catalyst was conducted at 650 °C for 24 h. As shown in Fig. 4, in the initial stage, the activity of the three catalysts is as follows: 2Ru → 15Ni > 2Ru > 15Ni, which is agreed with the results in the activity test. Overall, all the catalysts undergo deactivation along with the reaction time. In the case of the monometallic catalysts, the hydrogen yield drops significantly for the whole test period. 2Ru shows better activity than 15Ni within 12 h, while suffers a significant decrease in hydrogen yield during the latter 12 h, indicating the worst stability of 2Ru. However, the bimetallic 2Ru → 15Ni catalyst maintains its activity much better than the monometallic catalysts, with only a 7% decrease in the hydrogen yield within 18 h. At the end of the durability test, 2Ru → 15Ni keeps the highest hydrogen yield (33.2%) than those of 2Ru (5.8%) and 15Ni (14.3%), indicating that the loading of both 2Ru and 15Ni not only enhances the activity of the catalysts but also strengthens the catalyst stability tremendously.

Accordingly, the yields of carbonaceous gas over 2Ru → 15Ni are much higher than those of 15Ni and 2Ru. For the 2Ru → 15Ni catalyst, only 11.4% of unreacted oil was detected in liquid within 18 h. However, for 15Ni and 2Ru, 46.4% and 37.4% of unreacted oil were detected only within 6 h, respectively. This also indicates the much better stability of the bimetallic catalyst than the monometallic catalysts.

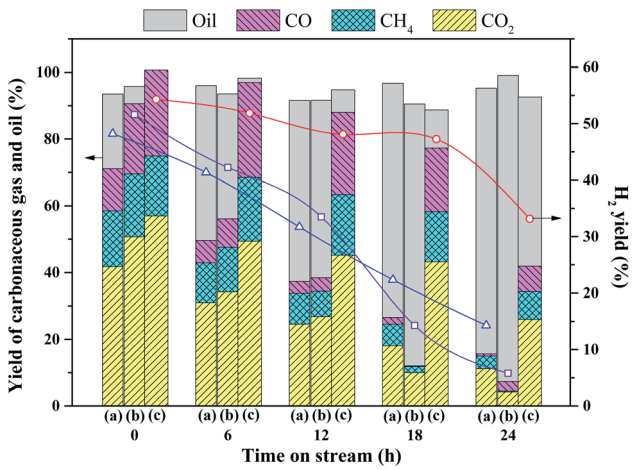

Fig. 4 Yields of hydrogen, carbonaceous gas, and oil in the steam reforming of xylene as a function of time on stream over (a) 15Ni, (b) 2Ru, and (c) 2Ru → 15Ni. Reaction conditions: WHSV = 20.8 h^{-1}, S/C = 3.4, 650 °C, 1.0 MPa.

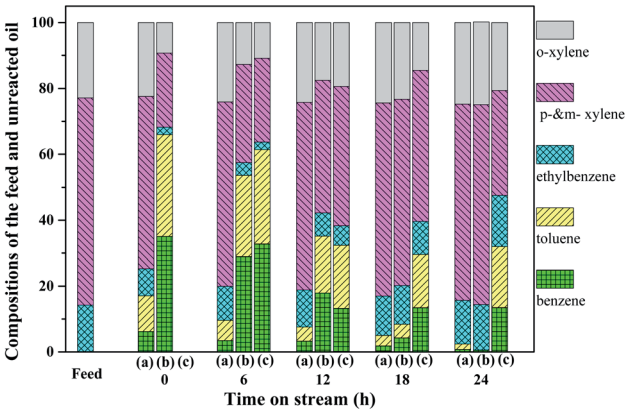

Fig. 5 Oil compositions as a function of time on stream in the steam reforming of xylene over (a) 15Ni, (b) 2Ru, and (c) 2Ru → 15Ni. Reaction conditions: WHSV = 20.8 h^{-1}, S/C = 3.4, 650 °C, 1.0 MPa.

The feed and unreacted oil at different times on stream of the durability test were analyzed by GC-FID. The feed consists of *o*-xylene (22.8%), *p*- & *m*-xylene (62.9%), and ethylbenzene (14.2%), which have various reactivities over these three catalysts. As shown in Fig. 5, the content of *o*-xylene does not change over the 15Ni catalyst in comparison to the feed, while the conversions of *p*- & *m*-xylene and ethylbenzene are observed, indicating that *o*-xylene has lower reactivity than *p*- & *m*-xylene and ethylbenzene, which is probably attributed to the steric and electronic effects.[4] During the durability, the compositions of *o*- & *p*- & *m*-xylenes and ethylbenzene decrease, while the formation of toluene and benzene is observed, revealing that some side reactions such as demethylation and C–C cracking of the ethyl group may occur. The compositions of toluene and benzene also decrease with the reaction time, indicating that the catalyst deactivation also slows the reactions to form toluene and benzene. This means that both the steam reforming and the side reactions are catalyzed by the catalysts. Particularly, at 12, 18, and 24 h, the compositions of toluene and benzene over 2Ru → 15Ni are much higher than those over 15Ni and 2Ru, suggesting that the 2Ru → 15Ni catalyst also have the best catalytic performance towards the demethylation of aromatics due to the superior C–C cleavage of metallic Ni–Ru clusters. For 15Ni, the conversions of *p*- & *m*-xylene and ethylbenzene, as well as the production of toluene and benzene, decrease with the reaction time, indicating that the catalyst suffers from deactivation. For the 2Ru catalyst, all the compositions in the feed are converted and a large amount of toluene and benzene is produced in the initial stage of the test, suggesting that 2Ru has a better catalytic performance than 15Ni. On the other hand, the conversion of reactants and the yield of products decrease with reaction time because of the deactivation of 2Ru. In contrast, the 2Ru → 15Ni catalyst shows an

excellent catalytic performance towards all the compositions in the feed, with nearly complete conversions in the initial stage of the durability test, indicating that the bimetallic catalyst has better adaptability in catalyzing various aromatic compounds.

3.1.4 Coke formation. The coke amount, BET surface area, and pore volume of the catalysts before and after reaction are listed in Table 1. After a 24 h durability test, the 15Ni catalyst has the most coke, reaching 0.518 g g_{cat}^{-1}, indicating that coke forms easily on the Ni-based catalyst. For the 2Ru catalyst, the coke amount decreases to 0.462 g g_{cat}^{-1}. The 2Ru → 15Ni catalyst exhibits the best coke resistance with a coke amount of 0.365 g g_{cat}^{-1} due to the addition of Ru. Ru was found to help curb the coke deposition by changing the surface reactions.[37] The coke formation is also related to the activity and stability of the catalyst. The high activity and stability facilitate the instant conversion of the feed into gaseous products, thus less coke precursor will accumulate on the active sites. Consequently, the coke resistance of the catalyst shows the same trend with the catalyst activity and stability, decreasing as follows: 2Ru → 15Ni > 2Ru > 15Ni. The carbon species formed on the catalyst were further determined by TGA and the DTG profiles of the spent catalysts are presented in Fig. 10. The positive peaks at low temperatures are associated with the oxidation of Ni and the negative peaks at about 600 °C are due to the coke combustion. The peak area represents the amount of the formed coke on the catalyst. It is shown that the coke amount decreases in the following trend: 15Ni > 2Ru > 2Ru → 15Ni-750. The coke combustion peaks of all the catalysts are centered at 600 °C originating from graphitic carbon,[38] indicating a similar coke formation mechanism.

Both the surface area and the pore volume of these coked catalysts decreased to a much low level, indicating that a large portion of pores is obstructed by the coke deposition after the durability test. The pore volume of the coked catalyst decreases in the following trend: 2Ru → 15Ni > 2Ru > 15Ni, which are attributed to the various coke depositions of the three catalysts. The pore size distribution of the fresh, coked, and decoked catalyst is shown in Fig. 6. Compared to the fresh catalysts, the pore diameter of the coked catalysts shifts to larger values, indicating that the small-sized pores are blocked by the coke deposition, meanwhile, some large-sized pores are formed. After the decoking procedure, the surface areas increase but are still lower than those of the fresh catalysts. As shown in Fig. 6, the proportion of small-sized pores in the decoked catalyst is less than that of the fresh catalyst, while the large-sized pore is more, indicating that a portion of the small-sized pores collapses, forming some larger ones during the reaction and calcination process. This process is irreversible, leading to the sintering of the active metals on the catalyst.

3.2 Effect of loading sequence of active metals

The effect of the loading sequence of active metals on the catalytic performance of the bimetallic catalyst was investigated by loading the active metals sequentially (15Ni → 2Ru, 2Ru → 15Ni) and simultaneously (2Ru ↔ 15Ni). The pore size distribution of the catalysts with various loading sequences is shown

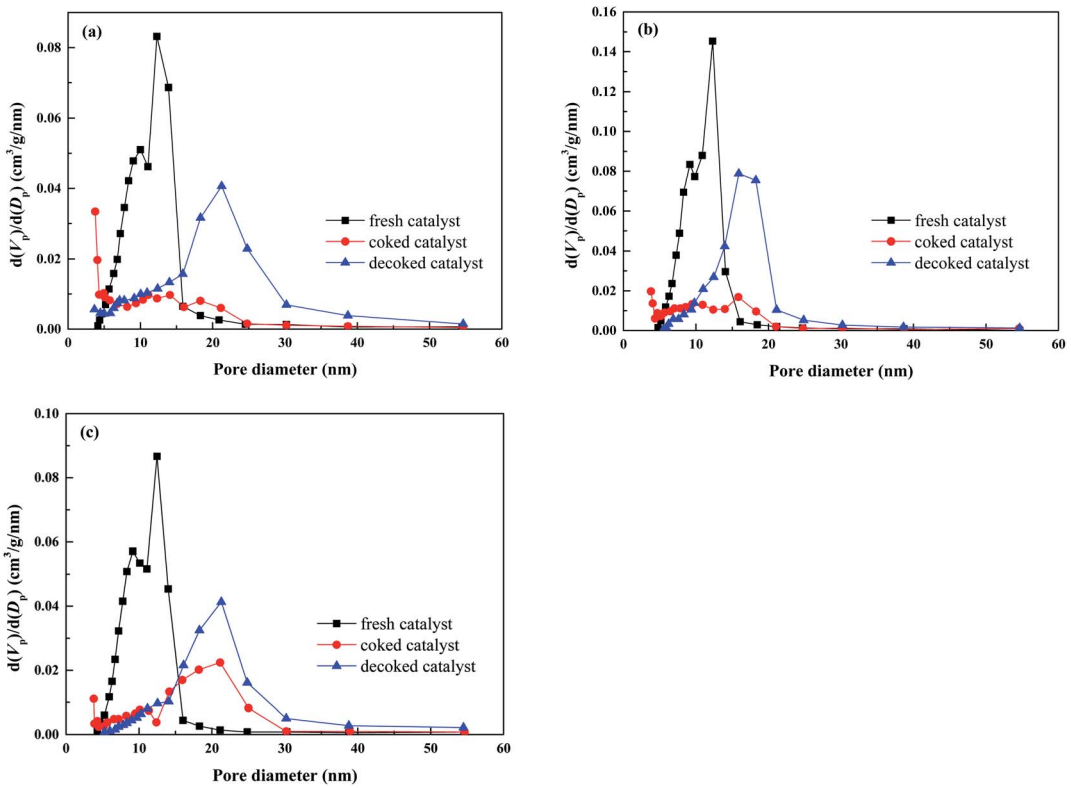

Fig. 6 Pore size distribution of the fresh, coked, and decoked catalysts. (a) 15Ni, (b) 2Ru, and (c) 2Ru → 15Ni.

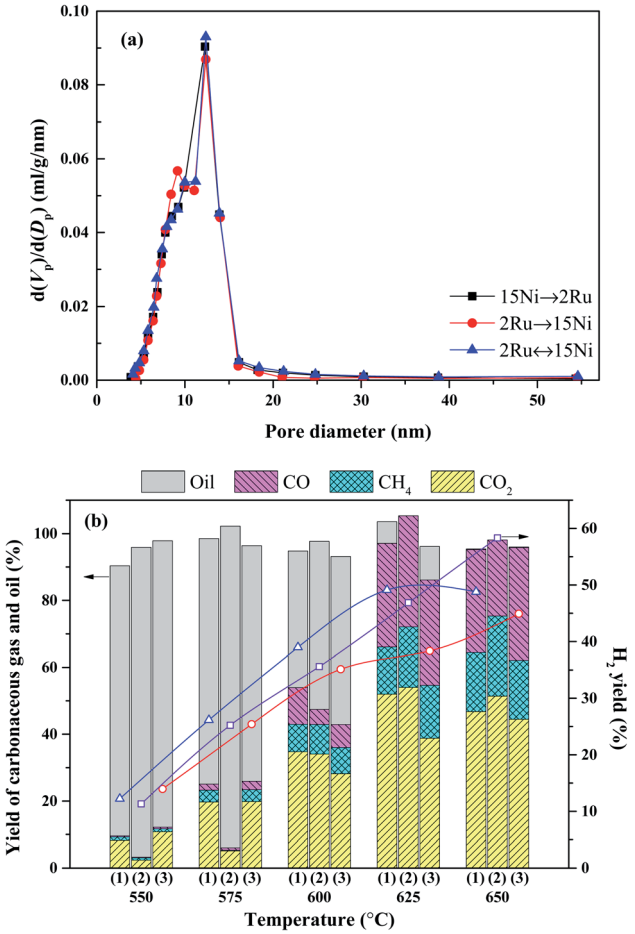

Fig. 7 (a) Pore size distributions of the reduced catalysts; (b) yields of hydrogen, carbonaceous gas, and oil in the steam reforming of xylene under various reaction temperatures over (1) 15Ni → 2Ru, (2) 2Ru → 15Ni, and (3) 2Ru ↔ 15Ni. Reaction conditions: WHSV = 20.8 h^{-1}, S/C = 3.4, 1.0 MPa.

in Fig. 7a. No significant distinction is observed in their pore distribution. However, 2Ru → 15Ni maintains more small-sized pores centered at 9 nm than 15Ni → 2Ru and 2Ru ↔ 15Ni, indicating that the loading sequence affects the proportion of small-sized pores. The first loading of Ru to the catalyst can inhibit the further penetration of Ni to the small-sized pores, which may be favorable to the adsorption of reactants on the catalyst. As shown in Fig. 7b, the loading sequence of the active metals significantly affects the activity of catalysts at different temperatures. For the sequentially loading catalysts, below 600 °C, 15Ni → 2Ru shows better catalytic performance than 2Ru → 15Ni, with much higher oil conversion and hydrogen yield. On the contrary, above 625 °C, 2Ru → 15Ni shows better catalytic performance than 15Ni → 2Ru. This may be explained by the sintering of Ni during the reaction, which reduces the formed Ni–Ru clusters. It is reported that the high activity and stability of NiRu bimetallic catalyst is owing to the formation of Ni–Ru clusters.[16] For the 15Ni → 2Ru catalyst, as shown in Scheme 1a, the first loading of Ni obstructs the small-sized pore and the Ni–Ru cluster mainly forms on the surface of Ni. The reactants can be easily adsorbed on the more active Ni–Ru sites, thus 15Ni → 2Ru shows better performance at low temperatures. However, at high temperatures, Ni with a large loading amount will undergo sintering, which leads to the low dispersion of the Ni–Ru sites. On the contrary, for 2Ru → 15Ni, as shown in Scheme 1b, the first loading of Ru makes the Ni–Ru cluster mainly form in the small-sized pore and the sintering of Ni cannot affect the dispersion of Ni–Ru sites significantly. Although the coverage of Ni will lead to the difficult diffusion at low temperatures, showing a worse performance than 15Ni → 2Ru, the maintained Ni–Ru sites play a crucial role in catalyzing the reaction at high temperatures, thus 2Ru → 15Ni shows a much higher hydrogen yield (58.3%) than that of 15Ni → 2Ru (48.7%) at 650 °C. However, the simultaneous loading catalyst 2Ru ↔ 15Ni shows the lowest activity because portions of the formed Ni–Ru sites are covered by a large amount of Ni before the reaction, as shown in Scheme 1c. Therefore, the loading sequence of 2Ru → 15Ni is best fitted for the steam reforming reaction owing to the maintenance of the formed Ni–Ru sites at high temperatures.

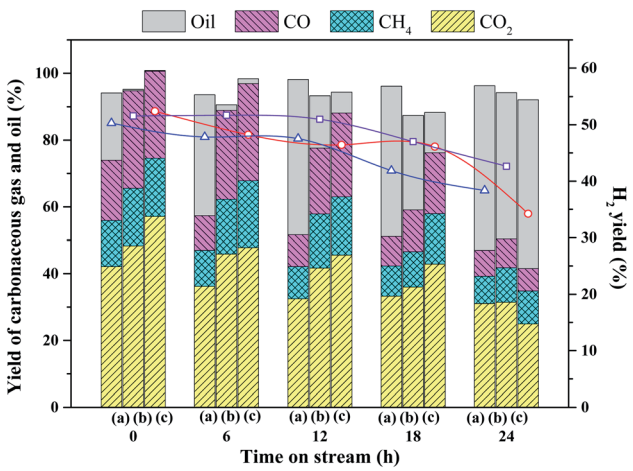

Fig. 8 Yields of hydrogen, carbonaceous gas, and oil in the steam reforming of xylene as a function of time on stream over the catalyst calcined at (a) 1100 °C, (b) 1000 °C, and (c) 750 °C. Reaction conditions: WHSV = 20.8 h^{-1}, S/C = 3.4, 650 °C, 1.0 MPa.

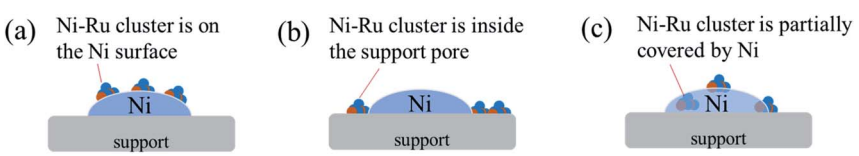

Scheme 1 The possible state of Ni–Ru clusters on the catalyst of (a) 15Ni → 2Ru, (b) 2Ru → 15Ni, and (c) 2Ru ↔ 15Ni.

Table 2 Coke amount, BET surface area, and pore volume of the catalysts with various calcination temperatures

Catalyst		Surface area (m^2 g^{-1})	Pore volume (cm^3 g^{-1})	Coke (g g_{cat}^{-1})
2Ru → 15Ni – 750 °C	Fresh	151	0.497	0.365
	Coked	65.5	0.302	
	Decoked	74.6	0.463	
2Ru → 15Ni – 1000 °C	Fresh	83.5	0.460	0.166
	Coked	71.5	0.404	
	Decoked	82.5	0.451	
2Ru → 15Ni – 1100 °C	Fresh	61.6	0.341	0.329
	Coked	51.6	0.275	
	Decoked	60.2	0.332	

3.3 Effect of support calcination

The 2Ru → 15Ni catalysts calcined at 750 °C, 1000 °C, and 1100 °C were tested at 650 °C for 24 h and the results are presented in Fig. 8. In the initial stage, the catalysts calcined at 750 °C and 1000 °C show high catalytic activity, with almost complete oil conversions. The catalyst calcined at 1100 °C shows low activity, with a conversion of only 79.8%. This is related to the change of the porous structure on the support at various calcination temperatures. As shown in Table 2, the surface area and pore volume of the fresh catalyst decrease with the increasing calcination temperature due to the collapse of pores in the support. The fresh catalyst calcined at 750 °C has a high surface area up to 151 m^2 g^{-1}, which facilitates the dispersion of active metals on the support. The low surface area of the catalyst calcined at 1100 °C (61.6 m^2 g^{-1}) leads to the poor dispersion of active metals. Thereby, the catalyst calcined at 750 °C shows the best activity while the catalyst calcined at 1100 °C shows the lowest activity in the initial stage. Although the surface area of the catalyst calcined at 1000 °C is lower (83.5 m^2 g^{-1}) than that of the catalyst calcined at 750 °C, the pores in the catalyst calcined at 1000 °C still provide enough surface for the dispersion of active metals. Therefore, the catalyst calcined at 1000 °C still shows excellent activity in the initial stage. Nevertheless, the catalyst calcined at 750 °C suffers from a distinct activity drop along with the reaction time and shows the lowest oil conversion and hydrogen yield after 24 h because of the pore collapse. In contrast, the catalysts calcined at 1000 °C and 1100 °C have much better stability, indicating that the high calcination temperature enhances the catalyst stability. As shown in Fig. 6c, most of the small-sized pores in 2Ru → 15Ni calcined at 750 °C are lost during the reaction and cannot be recovered by decoking, which leads to the coverage of the active sites on the catalyst. However, high calcination temperature can pre-collapse partial pores before reaction and enhance the hydrothermal stability during the reaction. As shown in Fig. 9, only a small number of pores in the catalysts calcined at 1000 °C and 1100 °C are lost in the steam reforming reaction, indicating that most of the small-sized pores are pre-collapsed before reaction and this enhances the stability of the support during the reaction. Therefore, the excellent stability of catalyst calcined at 1000 °C and 1100 °C is owing to the collapse of the small-sized pores before the loading of the active metals at high temperatures. However, the high calcination temperature decreases the surface area, leading to a low dispersion of the active metal, which is unfavorable to the catalytic activity. The catalyst calcined at 1000 °C well balances the active metal dispersion and the support stability, showing the highest activity and stability. The coke formed on the catalyst after the durability test is shown in Table 2. Consistent with the results of the durability test, 0.365 g g_{cat}^{-1} of coke is formed on the catalyst calcined at 750 °C, while only 0.166 g g_{cat}^{-1} of coke is observed on the catalyst calcined at 1000 °C. The excellent coke resistance of the catalyst calcined at 1000 °C is

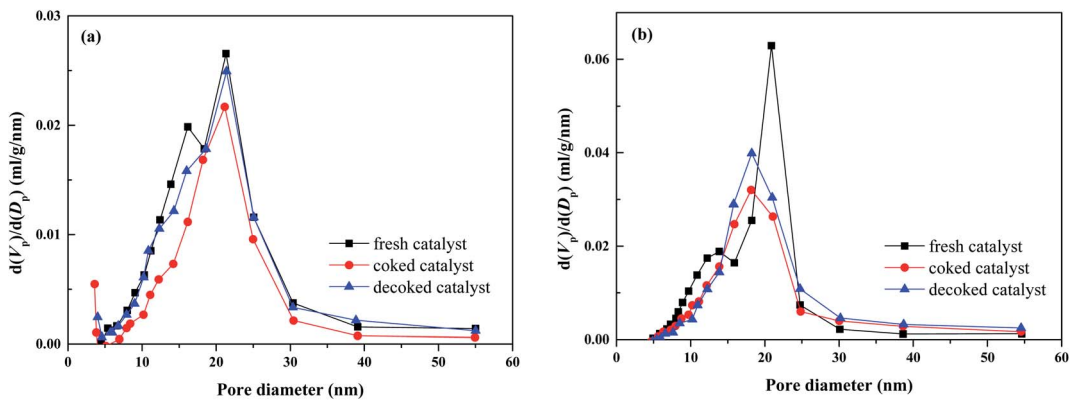

Fig. 9 Pore size distribution of the fresh, coked, and decoked catalysts calcined at (a) 1000 °C and (b) 1100 °C.

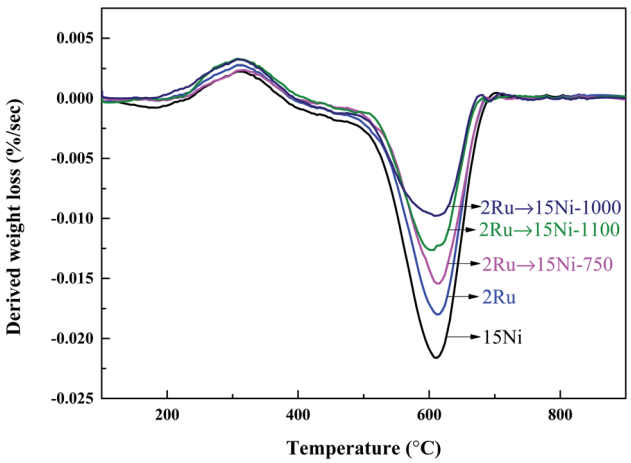

Fig. 10 DTG profiles of the spent catalysts after durability tests.

attributed to its high dispersion of active metals as well as the excellent stability of the support. As shown in Fig. 10, the carbon combustion peaks of all the samples are centered at 600 °C, which is associated with graphitic carbon,[38] revealing that the calcination temperature of the support has no significant influence on the carbon formation mechanism. After decoking, most of the obstructed pores in the catalysts calcined at 1000 °C and 1100 °C are recovered, while the surface area of the catalyst calcined at 750 °C decreases from 151 $m^2\ g^{-1}$ to 74 $m^2\ g^{-1}$, indicating that the catalyst stability is poor and many pores are lost under the severely hydrothermal environment.

4. Conclusions

The bimetallic catalyst 2Ru → 15Ni/La_2O_3–MgO–Al_2O_3 with high activity and stability in the steam reforming of xylenes was developed. The 15Ni catalyst has an advantage in catalyzing the reaction below 600 °C while the 2Ru catalyst has an advantage above 600 °C. The bimetallic 2Ru → 15Ni catalyst well combines the advantages of 15Ni and 2Ru, showing much higher activity than the monometallic catalysts, owing to the synergic effect between Ni and Ru. Both the two monometallic catalysts lost their activity after a 24 h durability test while the bimetallic catalyst shows excellent stability with the least coke formation. This indicates that the synergic effect between Ni and Ru not only improves the catalytic activity but also strengthens the catalyst stability. By analyzing the compositions of the unreacted oil, it is shown that *o*-xylene has the lowest reactivity due to the electronic and steric effects. Besides the steam reforming reaction, the demethylation and C–C bond cracking also occur. 15Ni → 2Ru shows better activity below 600 °C, while 2Ru → 15Ni shows much better activity above 600 °C because of the agglomeration of Ni–Ru clusters caused by the Ni sintering. The high calcination temperature strengthens the catalyst stability by pre-collapsing the small-sized pores but decreases the dispersion of the active metals. The catalyst calcined at 1000 °C well balances the active metal dispersion and support stability, showing the highest activity, best stability, and least coke formation. The carbon formed on the catalysts pertains to graphitic carbon and no significant changes in the carbon species are observed over various catalysts.

Conflicts of interest

There are no conflicts to declare.

Acknowledgements

The authors would like to acknowledge the funding supports obtained from Scientific Research Foundation of Jiaxing University (No. 70518058) and the Natural Science Foundation of Zhejiang Province, China (Grant No. LQ20B060008).

References

1 B. Tanç, H. T. Arat, E. Baltacıoğlu and K. Aydın, *Int. J. Hydrogen Energy*, 2019, **44**, 10120–10128.
2 Y. Manoharan, S. E. Hosseini, B. Butler, H. Alzhahrani, B. T. Senior, T. Ashuri and J. Krohn, *Appl. Sci.*, 2019, **9**, 2296.
3 Z. Wang, C. Wang, S. Chen and Y. Liu, *Int. J. Hydrogen Energy*, 2014, **39**, 5644–5652.
4 J. Pu, T. Toyoda and E. W. Qian, *Energy Fuels*, 2018, **32**, 1804–1811.
5 J. Pu, F. Ikegami, K. Nishikado and E. W. Qian, *Int. J. Hydrogen Energy*, 2017, **42**, 19733–19743.
6 J. Pu, K. Nishikado, N. Wang, T. T. Nguyen, T. Maki and E. W. Qian, *Appl. Catal., B*, 2018, **224**, 69–79.
7 M. Artetxe, J. Alvarez, M. A. Nahil, M. Olazar and P. T. Williams, *Energy Convers. Manage.*, 2017, **136**, 119–126.
8 L. Soler, A. Casanovas, J. Ryan, I. Angurell, C. Escudero, V. Pérez-Dieste and J. Llorca, *ACS Catal.*, 2019, **9**, 3641–3647.
9 C. Huck-Iriart, L. Soler, A. Casanovas, C. Marini, J. Prat, J. Llorca and C. Escudero, *ACS Catal.*, 2018, **8**, 9625–9636.
10 S. Bepari and D. Kuila, *Int. J. Hydrogen Energy*, 2020, **45**, 18090–18113.
11 S. Ogo and Y. Sekine, *Fuel Process. Technol.*, 2020, **199**, 106238.
12 G. Chen, J. Tao, C. Liu, B. Yan, W. Li and X. Li, *Renewable Sustainable Energy Rev.*, 2017, **79**, 1091–1098.
13 J. Pu, Y. Luo, N. Wang, H. Bao, X. Wang and E. W. Qian, *Int. J. Hydrogen Energy*, 2018, **43**, 3142–3153.
14 E. Meloni, M. Martino and V. Palma, *Catalysts*, 2020, **10**, 352.
15 H. D. Demsash, K. V. K. Kondamudi, S. Upadhyayula and R. Mohan, *Fuel Process. Technol.*, 2018, **169**, 150–156.
16 A. Ishihara, E. W. Qian, I. N. Finahari, I. P. Sutrisna and T. Kabe, *Fuel*, 2005, **84**, 1462–1468.
17 Y. Im, J. H. Lee, B. S. Kwak, J. Y. Do and M. Kang, *Catal. Today*, 2018, **303**, 168–176.
18 M. Khzouz, E. I. Gkanas, S. Du and J. Wood, *Fuel*, 2018, **232**, 672–683.
19 C. Italiano, K. Bizkarra, V. L. Barrio, J. F. Cambra, L. Pino and A. Vita, *Int. J. Hydrogen Energy*, 2019, **44**, 14671–14682.
20 Z. Liu, F. Zhang, N. Rui, X. Li, L. Lin, L. E. Betancourt, D. Su, W. Xu, J. Cen, K. Attenkofer, H. Idriss, J. A. Rodriguez and S. D. Senanayake, *ACS Catal.*, 2019, **9**, 3349–3359.

21 C.-J. Pan, M.-C. Tsai, W.-N. Su, J. Rick, N. G. Akalework, A. K. Agegnehu, S.-Y. Cheng and B.-J. Hwang, *J. Taiwan Inst. Chem. Eng.*, 2017, **74**, 154–186.
22 L. He, S. Hu, L. Jiang, G. Liao, X. Chen, H. Han, L. Xiao, Q. Ren, Y. Wang, S. Su and J. Xiang, *Fuel Process. Technol.*, 2018, **176**, 7–14.
23 Z. Zhang, Y. Wang, K. Sun, Y. Shao, L. Zhang, S. Zhang, X. Zhang, Q. Liu, Z. Chen and X. Hu, *J. Energy Chem.*, 2020, **43**, 208–219.
24 Z. Zhang, Z. Ou, C. Qin, J. Ran and C. Wu, *Fuel*, 2019, **257**, 116032.
25 P. Feng, K. Huang, Q. Xu, W. Qi, S. Xin, T. Wei, L. Liao and Y. Yan, *Int. J. Hydrogen Energy*, 2020, **45**, 8223–8233.
26 D. S. Lima, C. O. Calgaro and O. W. Perez-Lopez, *Biomass Bioenergy*, 2019, **130**, 105358.
27 Z. Zhang, X. Zhang, L. Zhang, Y. Wang, X. Li, S. Zhang, Q. Liu, T. Wei, G. Gao and X. Hu, *Energy Convers. Manage.*, 2020, **205**, 112301.
28 M. Wang, F. Zhang and S. Wang, *Int. J. Hydrogen Energy*, 2017, **42**, 20540–20548.
29 M. Greluk, M. Rotko and S. Turczyniak-Surdacka, *Renewable Energy*, 2020, **155**, 378–395.
30 M. Dan, M. Mihet, Z. Tasnadi-Asztalos, A. Imre-Lucaci, G. Katona and M. D. Lazar, *Fuel*, 2015, **147**, 260–268.
31 M. Surendar, T. V. Sagar, B. H. Babu, N. Lingaiah, K. S. R. Rao and P. S. S. Prasad, *RSC Adv.*, 2015, **5**, 45184–45193.
32 S. Sang, Z.-J. Zhao, H. Tian, Z. Sun, H. Li, S. Assabumrungrat, T. Muhammad, L. Zeng and J. Gong, *AIChE J.*, 2020, **66**, e16877.
33 N. Alarcón, X. García, M. A. Centeno, P. Ruiz and A. Gordon, *Appl. Catal., A*, 2004, **267**, 251–265.
34 K. Kousi, D. I. Kondarides, X. E. Verykios and C. Papadopoulou, *Appl. Catal., A*, 2017, **542**, 201–211.
35 C. Mirodatos, H. Praliaud and M. Primet, *J. Catal.*, 1987, **107**, 275–287.
36 T. Suzuki, H.-i. Iwanami and T. Yoshinari, *Int. J. Hydrogen Energy*, 2000, **25**, 119–126.
37 H. Zhou, T. Zhang, Z. Sui, Y.-A. Zhu, C. Han, K. Zhu and X. Zhou, *Appl. Catal., B*, 2018, **233**, 143–159.
38 M. Chen, X. Li, Y. Wang, C. Wang, T. Liang, H. Zhang, Z. Yang, Z. Zhou and J. Wang, *Energy Convers. Manage.*, 2019, **184**, 315–326.